RESEARCH ARTICLE

An Integrated Framework for BIM Development of Concrete Buildings Containing Both Surface Elements and Rebar

ZHONGMING XIANG [ID]1, GE OU2, AND ABBAS RASHIDI3, (Member, IEEE)

1Stantec, Salt Lake City, UT 84121, USA
2Department of Civil and Coastal Engineering, University of Florida, Gainesville, FL 32603, USA
3Department of Civil and Environmental Engineering, The University of Utah, Salt Lake City, UT 84112, USA

Corresponding author: Zhongming Xiang (gary.xiang@stantec.com)

ABSTRACT As-built Building Information Models (BIM) are increasingly used to facilitate the management of all aspects of built infrastructure's life cycle. Existing studies mainly focus on automating as-built BIM development for surface elements but often ignore embedded elements such as rebar due to the inaccessibility with typical sensing devices, such as image-based or time-of-flight-based methods. To tackle the issue, this research utilizes Ground Penetrating Radar (GPR) together with the photogrammetry method to generate BIMs for in-service buildings considering both surface elements (e.g., column, slab, wall, etc.) and rebar. As the first step, as-built BIM for surface elements is generated and then existing rebar is identified by using GPR. A calibration label is designed and attached to elements which are scanned by GPR device, and a series of images are captured from those elements and then used with other images to generate point clouds. Faster RCNN is then utilized to recognize labels among all images. Next, an inverse photogrammetry approach is deployed to identify the scanned elements in BIM. By matching the recorded timestamps of GPR data and labeled images, links between the rebar in GPR data and elements in BIMs are successfully established. Finally, IFC (Industry Foundation Classes) is developed to generate as-built BIM models. Six case studies demonstrate that the system is capable of automatically developing as-built BIM, while embedded rebar could be efficiently localized and projected into corresponding elements in BIM.

INDEX TERMS As-built building information model, deep learning, GPR, industry foundation classes, inverse photogrammetry, point cloud, rebar placement.

I. INTRODUCTION

As a revolutionary and fast-growing technique in the last two decades, Building Information Modeling (BIM) is the process to generate 3D models with proprietary information for supporting decision-making within the architecture/engineering/construction/facility management (AEC/FM) industry and has been widely used to improve the levels of automation, efficiency, and productivity for various types of projects [1], [2]. The BIM-relevant investments are continuously increasing, and the global market is anticipated to reach USD 16.35 billion in 2025 [3]. The great demand for applications has promoted the research on BIM solutions, some of which have been designed as commercial programs,

The associate editor coordinating the review of this manuscript and approving it for publication was Kathiravan Srinivasan [ID].

such as Autodesk Revit, MicroStation, and ArchiCAD. However, operations of these tools are highly dependent on human intervention and cannot be used as a tool to generate BIM automatically. Therefore, researchers in the AEC industry are still working on innovative techniques to establish fully automated procedures for BIM development.

Currently, a large number of studies have been reported with various algorithms that are mainly focused on as-built BIM development for surface elements, such as shear walls, columns, slabs, and beams [4], [5], [6] from existing buildings. The automation issue has been successfully solved by existing studies. However, rebar, as an important reinforcement component for structural health monitoring and other applications, has always been ignored during the BIM development for in-service buildings, caused by the inaccessibility of current devices (i.e., camera or laser scanner)

IEEE *Access*

Z. Xiang et al.: Integrated Framework for BIM Development of Concrete Buildings Containing Both Surface Elements and Rebar

for the embedded rebar. For as-plan buildings, this issue can be solved as the spatial information of rebar can be directly extracted from drawings and converted to BIMs, but for in-service buildings, especially for those buildings with inadequate drawings, the issue turns to be significant and has no solutions in the AEC industry. Although some existing studies [7], [8], [9] have been conducted on this topic, most of them focus on exposed rather than embedded rebar.

To generate an as-built BIM with surface elements and rebar for in-service buildings, the following objectives should be achieved simultaneously: (1) a robust procedure of BIM development for surface elements (i.e., shear walls, columns, slabs, etc.), (2) an accurate algorithm of rebar identification identifying rebar's quantities, layouts, and depths from concrete elements, and (3) an automated pipeline of integrating rebar and as-built BIMs. Ground penetrating radar (GPR) provides the potential to accomplish these objectives as it can obtain rebar's spatial information by scanning concrete elements and has the possibility to build the link between rebar and scanned elements. A number of solutions have been suggested to address the first two objectives [10], [11], [12] and research in the third objective is still ongoing. Thus, to fill the gap, this paper proposes an innovative procedure to combine the as-built BIM development and rebar identification. The following sections will elaborate on the state-of-the-art research and practices in the related areas.

A. STATE-OF-THE-ART RESEARCH ON BIM DEVELOPMENT

To develop as-built BIM for surface elements, there are usually three steps: (1) data acquisition, which generates point clouds by acquiring spatial information of targets, (2) point cloud segmentation, which organizes unstructured point clouds for further processing by grouping similar points, and (3) BIM development from point clouds, which converts structured point clouds into BIM by recognizing element categories.

The objective of data acquisition is mainly to generate point clouds, and the approaches can be classified into two categories: image-based method and time-of-flight-based method. For the image-based method, targets are scanned by cameras at different angles and positions to capture a set of successive images or video frames, which are then processed to build 3D models [13], [14], [15], [16]. The process involves several advanced methods, such as camera calibration, feature extraction and matching, and multi-view triangulation. As a well-developed technology, the current research focus is mainly on improving the quality of generated point clouds [17], [18]. According to the selected devices, the image-based method can be divided as photogrammetry (using images to generate point clouds) and videogrammetry (using video frames to generate point clouds) [19], [20]. The time-of-flight (ToF)-based method directly obtains the spatial information of targets by recording the two-way travel time of a laser beam [21]. Compared with the image-based method, the ToF-based method is straightforward as point clouds can be

generated without any further processing. However, this technique is limited by the high cost of devices and the requirements of sophisticated techniques for operators.

Segmenting point clouds is to organize unstructured data in a more structured format for further processing. Current solutions of point cloud segmentation involve two major categories: (1) spatial relationship-based method and (2) machine learning-based method. For the spatial relationship-based method, the point distribution is used as the feature to segment point clouds by considering the orientation, curvature, distance, and so on. The representative methods are region growing plane segmentation algorithm [22], which uses the smoothness factor to extract surfaces, M-estimator Sample and Consensus [23], which repeatedly fits planes with randomly selected points until generating a proper surface, element shape detection [24], which segments points based on element shape (i.e., walls are vertical surfaces), the fusion of color and spatial data [25], which combines the color features and spatial features together, etc. For the machine learning-based method, there are two popular algorithms: k-means clustering [26], [27], which initially defines a set of center points and then updates the centers based on point distributions, and Hierarchical clustering [28], [29], which initializes each point as a group and then hierarchically increases the groups according to the distances between points.

Converting point clouds into BIM is the process of identifying element categories from point clouds with an efficient and automated approach. Current practice in the AEC industry focused on manually identifying elements from a point cloud with the help of a commercial application (i.e., Autodesk Revit), but this process is time-consuming, labor-intensive, and error-prone. Thus, the exploration in the academic area is still ongoing to establish a highly automated procedure for as-built BIM development. The existing solutions are mainly rule-based and can be classified into two categories based on the adopted rules: (1) using the element attributes and (2) using the spatial relationships between elements. For the first category, the element attributes (i.e., walls are vertical [30], [31], columns are vertical [32], and floor and ceilings are horizontal [33], [34], [35]) are identified from the segmented point clouds and used to recognize element types. For the second category, typical buildings are constructed with elements that commonly have spatial relationships (i.e., windows and doors are openings in walls [31], the top and bottom constraints of walls are floors and ceilings [4], [36], floors are lower than ceilings [33], and slabs, piers, and girders in bridges are from top to down [37]), which are always used as another popular approach to convert point clouds into BIM.

B. STATE-OF-THE-ART TECHNIQUES IN REBAR IDENTIFICATION USING GPR DATA

Rebar identification is a procedure to extract the spatial information of embedded rebar from concrete elements, such as walls, columns, and slabs. GPR is a common tool used to
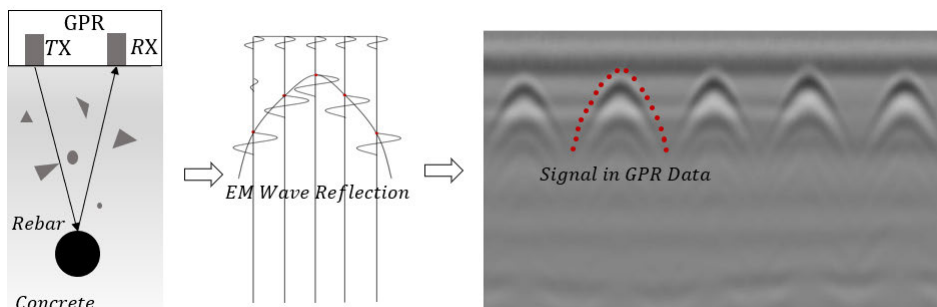
Z. Xiang et al.: Integrated Framework for BIM Development of Concrete Buildings Containing Both Surface Elements and Rebar

IEEE Access

FIGURE 1. Object detection using GPR data.

handle this task due to its portable size, high reliability, and ease of use [38]. An electromagnetic (EM) wave is generated by GPR and sent into the concrete element. It is reflected when reaching the surface of targets and then received by the GPR device. By recording the two-way travel time of the EM wave, rebar signals are reflected as hyperbolas in GPR data. Based on the geometrical features of the hyperbolas, we can calculate rebar's depths and sizes [39], [40]. Furthermore, a three-dimensional rebar arrangement can be determined by scanning both directions of an element. Figure 1 presents the principle of generating rebar signals in GPR data [10]. Thus, identifying rebar from GPR data is synonymous with processing hyperbolic patterns. Herein, two tasks should be addressed successively: rebar recognition which means identifying rebar signals in GPR data, and rebar localization which means determining the depths and sizes of rebar.

For rebar recognition, since rebar signals in GPR data are identical and have distinguishable characteristics compared with other signals (i.e., strong noise, cross rebar signal, and direct wave [10]), researchers have proposed a number of methods to recognize rebar according to this property, and existing studies can be classified as (1) machine learning-based method and (2) pattern-based method. For the machine learning-based method, the features of rebar signals are learned automatically from training datasets by algorithms and then used to recognize rebar from testing datasets. Some of the most popular methods, such as faster RCNN [41], [42], Naïve Bayes [43], and Support Vector Machine [44], are always adopted to recognize rebar in GPR data. However, this method is suffering a practical challenge in that a large amount of training and testing datasets are needed but are difficult to be collected. For the pattern-based method, rebar signals are directly analyzed to summarize a uniform rule that can be used for recognizing rebar from other GPR data. For example, Dou et al. [45] proposed a column-connection clustering (C3) algorithm to recognize rebar signals by decomposing hyperbolas vertically and clustering them based on the connections. There are some other similar studies, such as Zhou et al. [46] and Lei et al. [41]. However, the application of the pattern-based method is limited by the quality of GPR data as these methods are sensitive to the noise level.

For rebar localization, Bungey and H. [47] has stated that rebar depth and size determination is not a reliable application of GPR due to the inevitable noise, which blurs rebar signals dramatically. Nonetheless, researchers have already proposed some approaches, which can be classified as (1) software method that develops algorithms to directly derive rebar depth and size from GPR data [10], [48], and (2) hardware method that modifies the GPR device itself or integrates GPR device with other tools [46], [49]. However, both methods have significant limitations: the former is sensitive to noise, and the latter s high cost.

C. STATE-OF-THE-ART TECHNIQUES IN INTEGRATING REBAR AND BIM

After generating as-built BIM for surface elements and identifying the spatial information of rebars, another critical step is to translate rebars into corresponding elements in BIM, which means building 3D rebar with accurate coordinates. Vendors have launched some GPR devices equipped with 3D visualization software, such as Conquest 100 (Sensors and Software) and StructureScan (GSSI), but these devices have two major limitations: (1) pre-calibration patterns are needed to guild the scanning tasks [38]; and (2) manual processing is needed to integrate 3D rebars with BIM models as these tools are not compatible with BIM software. To solve the problems, researchers have been exploring a method that can automatically place rebar into corresponding elements in BIM [50], but it was focused on as-plan buildings as rebar information is extracted from 2D drawings. Thus, Xiang et al. [51] utilized GPR to detect concrete elements and converted the rebar information into corresponding elements in BIMs, which, however, were manually created in a commercial program.

D. GAPS AND RESEARCH OBJECTIVES

Summarizing the efforts contributed by researchers and practitioners, significant improvements in developing as-built BIMs with surface elements and rebar are still demanded to produce high fidelity industrial standard BIMs for as-built buildings. Existing studies on developing BIM models with rebar are mainly focused on three aspects: (1) generating

IEEE Access

Z. Xiang et al.: Integrated Framework for BIM Development of Concrete Buildings Containing Both Surface Elements and Rebar

rebar models during the construction phase [7], [8], which is not feasible for in-service buildings, (2) detecting exposed rebar [9], which ignores the embedded rebar, and (3) converting rebar from drawings into BIM models [52], which has the limitation of being applied in buildings without adequate drawings. To the best of our knowledge, there have been no prior works to automatically translate embedded rebar into corresponding elements in BIMs for in-service buildings. Integrating rebar and as-built BIMs is an active and ongoing research area.

Hence, this research will propose an automated solution to fill the gap. It will not only tackle the issue of embedding rebar in BIM but also enhance the automation level of BIM development with surface elements and rebar. To achieve the goals, the authors design the following three steps: (1) an algorithm consisting of an inverse photogrammetry approach and a deep learning method is proposed to develop as-built BIMs for surface elements; (2) a frequency filter-based method and a depth determination method are adopted to identify rebar's quantities, layouts, and depths from existing concrete buildings using GPR; and (3) a procedure for integrating rebar and as-built BIMs is creatively formulated by utilizing timestamps to connect rebar in GPR data and concrete elements with the help of a deep learning method, Faster RCNN. Additionally, this research introduces the *IFC* (Industry Foundation Classes) schema to generate models that are readable for various BIM platforms.

The difference of the proposed method and the existing studies is that the proposed method focuses on automatically integrating embedded rebar into BIM models for in-service buildings without the help of 2D drawings, while the existing studies focus on scanning exposed rebars [9] or generating rebar models from drawings [52]. The advantage of the proposed method is that it is highly automated and adaptive because of the utilization of deep learning method. It has the potential to be widely applied to the AEC industry to convert concrete buildings into BIM models containing rebar.

One major reason for selecting photogrammetry to develop BIM models is that a predefined label is used to mark scanned elements and recorded as images. To enhance the automation level, we select an image-based 3D modeling method that can merge these label images into the process of BIM development. In addition, photogrammetry is a mature technology and there are several commercially available photogrammetry-based software packages, such as RealityCapture, 3DF Zephyr, and ContextCapture. The last reason is that the associated costs of photogrammetry are lower than other 3D modeling technologies such as laser scanning [53].

The rest of this paper is organized as follows: Section II thoroughly discusses the proposed system of BIM development for surface elements and rebar; the experimental settings of six cases are presented in Section III; In Section IV, the results discussion corresponding to the six cases are illustrated; Section V conclude the accomplishments, limitations, and future works.

II. METHODOLOGY

As shown in Figure 2, the proposed solution of developing BIM with integrated surface elements and rebar for in-service buildings consists of three steps: (1) BIM development, (2) rebar identification, and (3) integration of rebar and BIM.

A. AS-BUILT BIM DEVELOPMENT FOR SURFACE ELEMENTS

To develop an as-built BIM, an innovative procedure by using inverse photogrammetry and a deep learning approach has been proposed and illustrated in Figure 3 [11].

(1) Point cloud generation, which is achieved by the photogrammetry method.

(2) Plane isolation, which is implemented by M-estimator sample consensus (known as MSAC [23], [54]) to cluster all points in the same plane.

(3) 3D to 2D projection, which utilized the inverse photogrammetry between 2D images and 3D models [51].

(4) 2D image segmentation, which is conducted by a deep learning method, DeepLab.

(5) Element identification, which is implemented based on the highest frequency of category among all points of the projected planes in 2D images.

B. REBAR IDENTIFICATION USING GPR DATA

Rebar identification is composed of rebar recognition in GPR data and rebar localization. Regarding rebar recognition, a frequency filter-based method to automatically recognize rebar signals in GPR data (Figure 4) has been proposed [12] based on two factors: (1) the signal directions between the spatial domain and the frequency domain have an angle of 90-degree [55], [56]; and (2) the signal interferences (direct wave, cross rebar signals, strong noise, and adjacent rebar signals) have different directions compared with expected rebar signals. According to these two factors, frequency filters can be designed to remove the signal interferences in the frequency domain. Meanwhile, the two tails of the hyperbola are also in two different directions, which can be used as a feature to recognize rebar signals in the frequency domain by using specifically designed filters.

Regarding rebar locations, two kinds of data should be determined: rebar depth and rebar size. For rebar depth, the negative correlation between the travel time of an EM wave and the maximum intensity of rebar signal in GPR data is utilized by slightly modifying the related parameters [12]). The initial relationship between EM wave and intensity has been widely applied to determine the deterioration conditions of rebar in concrete bridges [44], [57], but the performance of this application is limited due to the lack of high precision requirement. The authors have modified the negative correlation by proposing a correction intensity. For rebar size, rather than exploring a feasible approach, this research assumes 12.7 mm is the uniform diameter for all rebar since using GPR to determine rebar size is the least reliable application [47]. It should be noted that errors are not avoidable and always
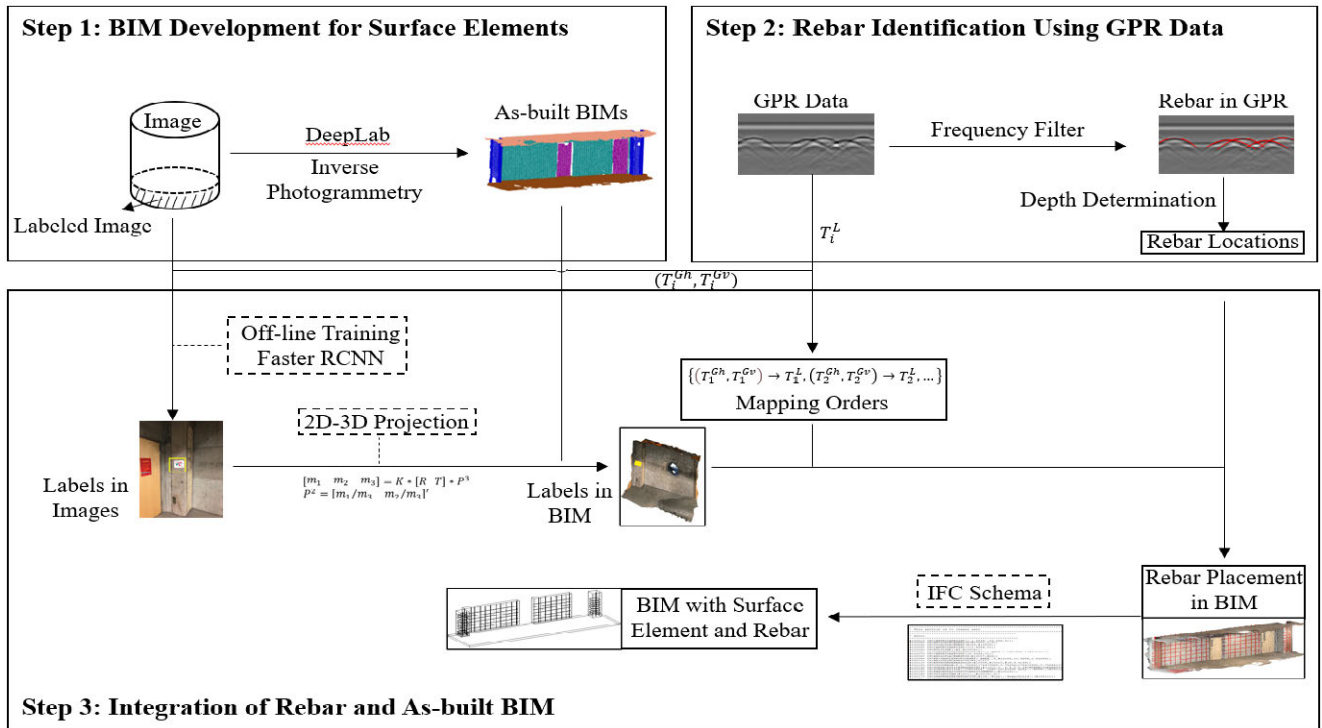
Z. Xiang et al.: Integrated Framework for BIM Development of Concrete Buildings Containing Both Surface Elements and Rebar

IEEE *Access*

FIGURE 2. The overall workflow of the proposed system.
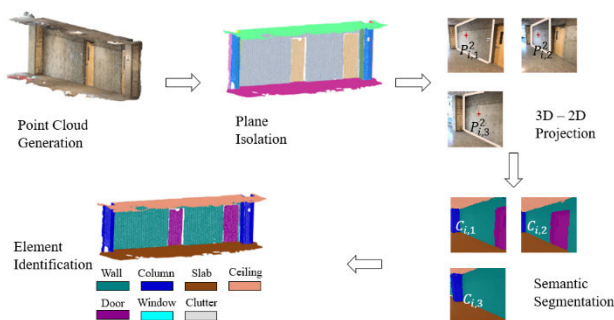
FIGURE 3. The workflow of as-built BIM development for surface elements.

FIGURE 4. Rebar recognition in GPR data: (a) raw GPR data, (b) recognized rebar.

FIGURE 5. Images with labels to indicate elements are scanned by the GPR device.

C. INTEGRATION OF REBAR AND AS-BUILT BIM

After acquiring as-built BIMs and spatial information of rebar, the following procedure is developed to integrate rebar information into as-built BIMs. To accomplish this goal, three sub-steps are developed in this section: (1) pairing the rebar in GPR data with their corresponding elements in BIMs, (2) inserting rebar into elements with accurate coordinates, and (3) generating BIM models that are compatible and readable with different platforms.

1) PAIRING REBAR DATA WITH ELEMENTS IN AS-BUILT BIM

The significant obstacle to pairing off the acquired rebar in GPR data and as-built BIMs is that GPR data does not contain any unique features that can map to a specific concrete element from which GPR data is obtained. Therefore, a practical solution is proposed by utilizing timestamps as an additional link. As shown in Figure 5, an extra image with a specifically
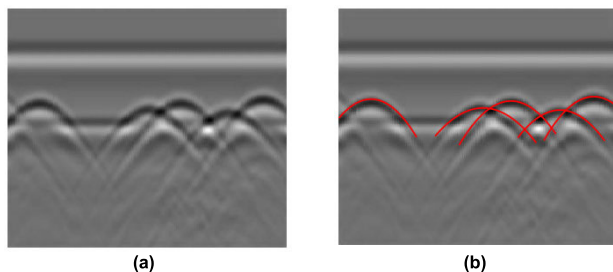
exist in BIM models. Nevertheless, errors can still fall within an acceptable range according to our previous studies [10].

IEEE Access

Z. Xiang et al.: Integrated Framework for BIM Development of Concrete Buildings Containing Both Surface Elements and Rebar

designed label is collected for each element and named as the labeled image. The sequence of collecting the labeled images is the same as scanning elements with the GPR device. According to the recorded timestamps, the labeled images and GPR data are grouped and matched one by one. The labeled images are later used to map the group data to the BIM.
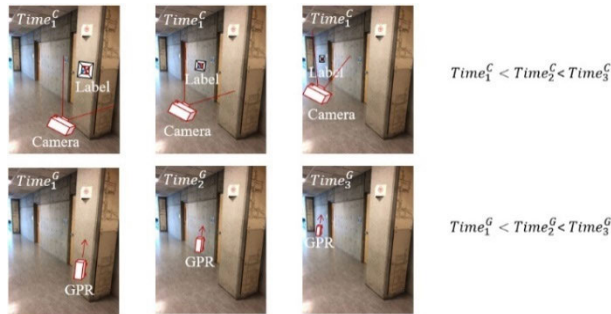

FIGURE 6. Same sequence of collecting GPR data and capturing labeled images.

a: TIMESTAMPS RECORDING

After collecting images for 3D reconstruction, a unique designed label is attached to each element scanned by the GPR device, and one image is acquired for each element. Meanwhile, the chronological sequences of the GPR data and the labeled images are recorded and used to match the scanned elements and GPR data automatically. In order to correctly match the GPR data and the labeled images, the labeled images are collected in the same order as the scanning sequence of the GPR device. For instance, the GPR device scans Element A first and then scans Element B, then the labeled image from Element A should be collected before Element B, which is illustrated in Figure 6.

(T_i^{Gh}, T_i^{Gv}) are the timestamps of GPR data scanned from the ith element E_i, Gh, Gv represent two directions of E_i. T_i^L is the timestamp of the labeled image collected from element E_i. As indicated above, the labeled images and the GPR data are collected in the same sequence, then an augmented rule can be designed as $\{(T_1^{Gh}, T_1^{Gv}) \rightarrow T_1^L, (T_2^{Gh}, T_2^{Gv}) \rightarrow T_2^L, \ldots\}$ to match the GPR data and the labeled images, which establishes the initial link between GPR data and scanned element.

b: LABEL RECOGNITION

The labeled images are served as bridges between the GPR data and the elements in BIM models. These labels, among all images, need to be detected and recognized first, furthermore, the 2D label images will need to be projected back to the 3D to indicate the scanned element in BIM models.

To implement label detection and recognition task, a deep learning method, Faster RCNN is introduced, which is a promising network for object detection due to three technical features: (1) an algorithm of selective search is designed to extract region proposals; (2) region proposals are converted

to feature maps; and (3) a region of interest pooling layer is added to rescale region proposals into a uniform size. Figure 7 illustrates the architecture of Faster RCNN.

The general idea of projecting 2D labels to 3D models is demonstrated in Figure 8, which applies the approach of inverse photogrammetry [58]. The photogrammetry is for 3D reconstruction by projecting 2D images into 3D models, while the inverse photogrammetry is to project 3D models back to 2D images. As discussed in [58], some intrinsic parameters of a pinhole camera are required to formulate the equations for projecting 3D points back to 2D images: (1) the calibration matrix K consisted of the principal point (x_0, y_0), the focal length (F_x, F_y) and the skew coefficient S_k (Equation 1), (2) the translation matrix T consisted of three intrinsic parameters (Equation 2), and (3) the rotation matrix R consisted of nine intrinsic parameters (Equation 3). Then, according to the workflow of a pinhole camera model [59], the projection between a 3D point P^3 and a 2D point P^2 can be built by using Equations 4-5, where m_1, m_2 and m_3 are the intermediate variables served as a medium between P^3 to P^2. These three variables are first determined by P^3 (Equation 4) and then used to derive P^2 (Equation 5). Since the range of the label has been detected in the previous step, there will be a binary value to indicate if P^2 is within the label range or not. If P^2 locates in the label range, P^3 can be determined as a point of the label in the 3D model. By searching all 3D points, the label can be completely identified in the 3D model (Figure 8).

$$K = \begin{bmatrix} F_x & S_k & x_0 \\ 0 & F_y & y_0 \\ 0 & 0 & 1 \end{bmatrix} \tag{1}$$

$$T = \begin{bmatrix} t_1 \\ t_2 \\ t_3 \end{bmatrix} \tag{2}$$

$$R = \begin{bmatrix} r_{11} & r_{12} & r_{13} \\ r_{21} & r_{22} & r_{23} \\ r_{31} & r_{32} & r_{33} \end{bmatrix} \tag{3}$$

$$\begin{bmatrix} m_1 & m_2 & m_3 \end{bmatrix} = K * [RT] * P^3 \tag{4}$$

$$P^2 = \begin{bmatrix} m_1/m_3 & m_2/m_3 \end{bmatrix}' \tag{5}$$

2) REBAR PLACEMENT IN CORRESPONDING ELEMENTS

Next, rebars are translated from GPR data into corresponding elements in BIM with accurate coordinates. As shown in Figure 9, each element is scanned in two directions with two separated GPR scans, and we take the vertical rebar (see the left scan in Figure 9) as the example to discuss the rebar placement. In order to reduce the influence of depth deviations within one element and simplify the procedure, we assume that all rebars in the same direction have a uniform depth. Although differences between detected and designed depths cannot be avoided due to the existence of construction errors, it still can fall within an acceptable error range. Some experiments have been conducted in [10], which indicates a mean average error of 6.73% for depth determination. It is
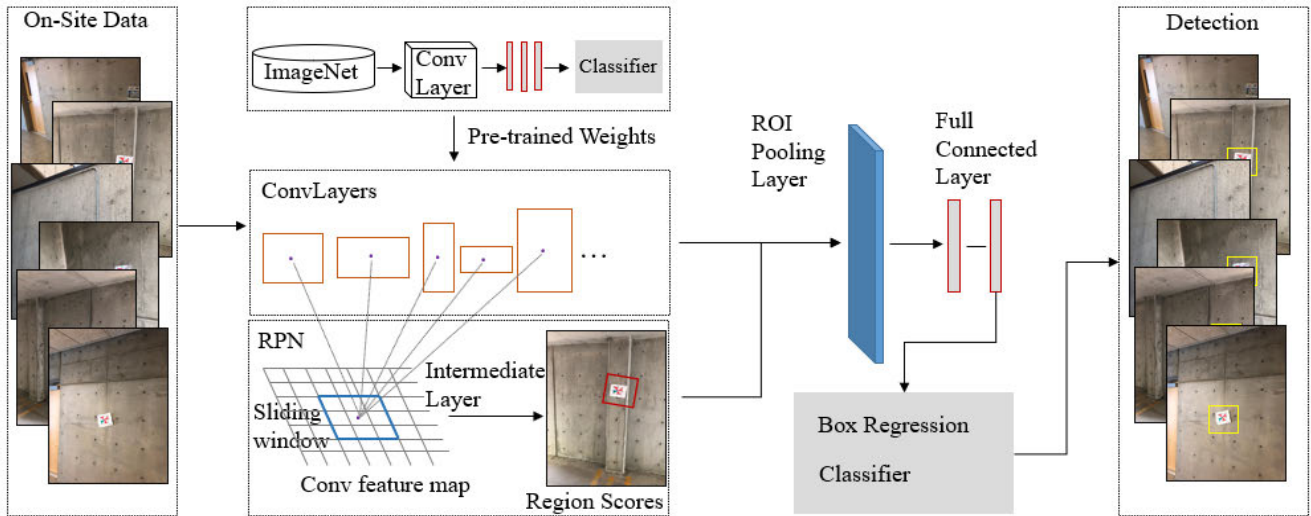
Z. Xiang et al.: Integrated Framework for BIM Development of Concrete Buildings Containing Both Surface Elements and Rebar

IEEE Access

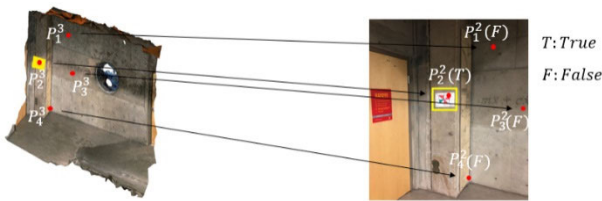**FIGURE 7.** The architecture of Faster RCNN.

FIGURE 8. Label projection from 2D image to 3D model.

indicated as D_G in GPR data with the unit of the pixel. Then, the rebar depths D_r in the BIM can be determined by Equation 6:

$$D_r = D_G/H_G * D_{max} \qquad (6)$$

where D_G is the pixel depth of GPR data, and D_{max} is the maximum detection depth of the GPR device. It is worth to noting that this procedure can be applied to concrete elements with any depths as it does not dependent on element sizes. Even though, the proposed method will not work if the embedded depth of rebar is greater than D_{max}.
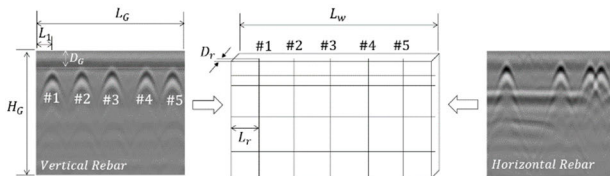
FIGURE 9. Rebar translation from GPR data into BIM.

Similarly, the distance from rebar i to the vertical element boundary is calculated by Equation 7:

$$L_r = L_i/L_G * L_w \qquad (7)$$

where L_i is the pixel distance between rebar i and the left boundary of GPR data, L_G is the pixel length of GPR data, and

L_w is the length of the element. The underlying reason behind this calculation is that although GPR data does not record the actual scanned lengths in concrete elements, but the length of GPR data is proportionate to the length of scanned element. In addition, each GPR data is scanned from left to right and bottom to top for each element, so the rebar complies with the same rule when being placed in BIM.

D. IFC-BASED BIM GENERATION

To generate as-built BIM that is compatible with various commercial applications, this research adopts the *IFC* to convert the point clouds with rebars into as-built BIM. It should be noted elements involved at this stage are walls, columns, slabs, and rebars, and other elements are not considered. The instances of *IFC* used in this research are *IfcWallStandarCase, IfcColumn, IfcSlab, and IfcReinforcingBar*. Meanwhile, this research detects the openings (i.e., doors, windows, or empty spaces) to vertically split shear walls, which are scanned by the GPR device. Besides the geometrical parameters, materials are also important features that must be identified. Nevertheless, material identification is not the scope of this research, thus, a set of predefined materials is applied to all elements.

In this research, we create a script to predefine all possible elements, such as walls, columns, slabs, and rebar. As discussed above, we consider the spatial details of models, thus, the quantities, locations, and scales of all elements are set as variables. After implementing the method, these variables are determined and fed into the predefined script to generate a file in *IFC* format, which can be read by cross-platform applications. Figure 10 shows the necessary workflow for generating *IFC* models.

III. EXPERIMENTAL SETUP

We select six case studies to evaluate the feasibility of the proposed system. Figure 11 shows the five concrete
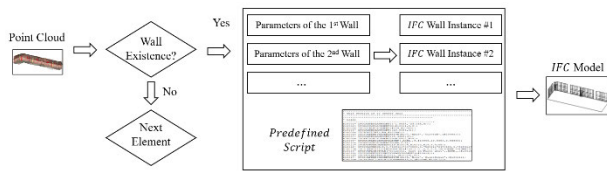
IEEE Access·

Z. Xiang et al.: Integrated Framework for BIM Development of Concrete Buildings Containing Both Surface Elements and Rebar

FIGURE 10. Generating IFC models.

	Case 1	Case 2	Case 3	Case 4	Case 5	Case 6
Building Code	MCE	MCE	LSND	FMAb	CRCC	BPLS
Shear Wall #	2	5	2	2	7	3
Column #	2	2	0	0	0	3
Slab #	1	1	1	0	1	1
Door #	2	3	0	0	1	0
Window #	0	4	0	0	5	0
Image Number	205	711	477	324	658	590
Label Images	5	8	4	2	4	2
GPR Scans	10	16	8	4	8	4

buildings, which are all located on the University of Utah. Case #1 and #2 is from a renovated building, MCE Building, which hosts the Department of Civil and Environmental Engineering; Case #3 is from a student living center, LSND building; Case #4 is from the FMAB buildings, which hosts the Department of Film and Media Arts; Case #5 is from the CRCC buildings used for business education; and Case #6 is from the BPLS building, a five-story parking lot. Table 1 summarizes the number of elements categories, image numbers, and GPR scans of the involved five cases.
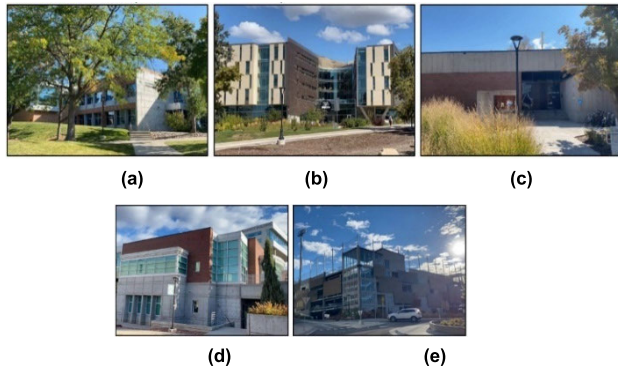
FIGURE 11. The profiles of the selected concrete buildings: (a) MCE Building, (b) LSND Building, (c) FMAB Building, (d) CRCC Building, and (e) BPLS Building.

Table 1 shows that the number of GPR scans is twice the number of labeled images since each element is scanned in both directions to obtain rebar arrangements, while only one labeled image is captured for each element. To generate quality point clouds, the image number of each case varies according to the scale of the target: larger-scale needs more images, and vice versa. Another thing that should be mentioned is that rebars are collected from shear walls and columns, and other elements are not scanned by the GPR device since the element boundaries (i.e., slabs) are not capable to be determined automatically, or no rebar is embedded in elements (i.e., doors and windows).

Besides the images for 3D reconstruction, this research collects 300 labeled images to train the Faster RCNN. To achieve a better performance, data augmentation is applied to increase the size of the dataset by scaling, flipping, rotating, cropping, and translating the original images. At last, this research obtains 1500 images, in which 60% (900) images are used as the training dataset, 20% (300) images are the validation dataset, and the rest 20% (300) images are the testing dataset.

There are two data collection devices: the camera for capturing images and the GPR scanner for obtaining rebar information. For the camera, a smartphone's camera is adopted with a resolution of 3024×4032 pixels and a focal length of 4 mm. To develop quality point clouds, the angle deviation between two adjacent images is controlled less than $15°$. For the GPR scanner, Handy Search NJJ-105, manufactured from Japan Radio Co., Ltd, is adopted in this research. It has a central frequency of 1.5 GHz and a maximum detection depth of 30 cm. Meanwhile, to save the setting time of well-established algorithms, this research uses ContextCapture, a commercial program of Bentley, to implement the photogrammetry procedure for 3D reconstruction from images. In addition, the proposed system is designed and executed on a computer with the configurations of Intel i7-8700 processor, 64 GB memory, and NVIDIA GeForce RTX 2080 Ti graphics card.

IV. RESULTS AND DISCUSSION
By implementing the proposed system for all six case studies, the point clouds, the point clouds with embedded rebars, and the corresponding BIMs are generated and presented in Figures 12-14. In general, the point clouds for the six cases are of high quality (Figure 12). With the assistance of the as-built BIM development approach for surface elements and the rebar identification approach, rebars are correctly embedded into corresponding elements in point clouds (Figure 13). Meanwhile, as-built BIMs are successfully generated by *IFC* and readable by various BIM platforms. Figure 14 are the models shown in Autodesk Revit. The following sub-sections will discuss the performance of the proposed framework in detail.

A. AS-BUILT BIM DEVELOPMENT
The performance of the photogrammetry-based BIM development is discussed at first. A deep learning method, DeepLab, is involved in this workflow. To train DeepLab, we collected 1500 images and used 60% of the images as the training dataset, 20% of the images as the validation dataset, and the rest 20% as the testing dataset. The Intersection-Over-Union between the prediction and the ground-truth bounding boxes on the testing dataset can reach 0.95 for walls, 0.90 for columns, 0.95 for slabs, 0.92 for doors,

Z. Xiang et al.: Integrated Framework for BIM Development of Concrete Buildings Containing Both Surface Elements and Rebar

IEEE *Access*

TABLE 2. Element identification for six cases.

Case #		Shear Wall	Column	Slab	Door	Window
1	True #	2	2	1	2	0
	Identified #	2	2	1	2	0
2	True #	5	2	1	3	4
	Identified #	5	2	1	3	0
3	True #	2	0	1	0	0
	Identified #	2	0	1	0	0
4	True #	2	0	0	0	0
	Identified #	2	0	0	0	0
5	True #	7	0	1	1	5
	Identified #	7	0	1	0	4
6	True #	3	3	1	0	0
	Identified #	3	0	1	0	0

and 0.95 for windows. Regarding point cloud generation, Figure 12 illustrates that photogrammetry can obtain promising performance since all elements are successfully developed. As shown in Figure 13, and after preprocessing with noise removal and down-sampling algorithms, all models maintain high-quality levels without any outliers. Table 2 summarizes the element recognition performance for all cases. Overall, 39 out of 48 elements have been successfully identified. Unlike object recognition for 2D images, the outputs of our method for object recognition in point clouds are binary because of using the highest frequency of category as results. The major cause of the failed cases is due to the fact that such specific elements might not exist within the training dataset. In this research, we did not collect enough cases similar to the elements involved in this research, such as the circular windows in Case 2 (Figure 12b) the standalone column with black color in Case 6 (Figure 12f). Besides, the two columns in Case 6 are recognized as parts of walls since 1) the texture of these two columns are similar to walls and 2) the columns are too thin to be identified.

B. REBAR TRANSLATION FROM GPR DATA INTO BIM
As a fundamental step for translating rebar into as-built BIMs, the performance of label recognition using Faster RCNN is discussed here: The precision and recall of Faster RCNN on the testing dataset are shown in Figure 15. The results are acceptable since the design of label recognition is to identify scanned elements. Once a label is recognized within one element, the element can be successfully identified.

Then, Faster RCNN is applied to recognize labels from the images, which are used to reconstruct point clouds. The accuracy, denoted whether or not the label is recognized, reaches 100%. Figure 16 includes three examples of the recognized labels. One major reason behind the high performance is that images for 3D reconstruction relatively have low noise and are easy to be processed. Subsequently, the labels in images are converted to point clouds to show the scanned elements by using inverse photogrammetry. Similarly, all labels are correctly converted to corresponding elements in 3D models. The examples of converting labels from 2D images into 3D models are presented in Figure 17, which demonstrates that

the labels are successfully indicated in 3D models at proper locations. However, compared the labels between 2D images and 3D models, the labels in 3D models are not the same as the shapes and areas in images. This phenomenon is caused by the fact that this research uses the boxes predicted by Faster RCNN, rather than the labels in images, to conduct projecting labels in 3D models.

Consequently, by pairing timestamps according to the sequences of capturing data, the GPR data and the labeled images can be correctly matched. Since the labeled images have been completely linked with elements in BIMs, all links between GPR data and elements are built as well, which demonstrates that rebar can be connected with corresponding elements in BIMs.

C. REBAR PLACEMENT
This research evaluates the performance of placing rebar in BIMs from the aspects of relative depths of rebars in two different directions and distance between rebars in the same direction. One column model and one shear wall model with embedded rebars are selected to implement the evaluation and shown in Figure 18. Regarding the relative depth of rebar placement, this research uses the mean depths of all rebars in one direction as the value to insert rebars in BIMs. For both models, the depth distribution of rebars is consistent with the depths in the GPR data. Rebars that are placed deeper in BIM in one direction are relatively deeper in GPR data than the GPR data in the other direction. On the other hand, distances between different rebars in BIM are also consistent with the GPR data. As demonstrated in Direction 1 of the column model (Figure 19), the normalized distance vectors between rebars in the BIM model and the GPR data are expressed in Equations 8-9, respectively.

$$X^M = \left(x_1^M, x_2^M, x_3^M, x_4^M, x_5^M, x_6^M, x_7^M, x_8^M, x_9^M\right)$$
$$= (0.22, 0.13, 0.42, 0.36, 0.29, 0.39, 0.31, 0.48, 0.28) \quad (8)$$

$$X^G = \left(x_1^G, x_2^G, x_3^G, x_4^G, x_5^G, x_6^G, x_7^G, x_8^G, x_9^G\right)$$
$$= (0.25, 0.16, 0.39, 0.35, 0.26, 0.36, 0.31, 0.53, 0.26) \quad (9)$$

Then, the cosine similarity, a well-known measure to determine the similarity between two vectors, is adopted to calculate the similarity of the distances between rebars in the BIM model and the GPR data. As illustrated in Equation 10, $sim\left(X^M, X^G\right)$ reaches 0.99, which represents a high similarity as two vectors are more similar if the value is closer to 1, and vice versa. Thus, rebar placement in BIM models is consistent with the detection in GPR data. It is worth noting we directly use the element boundaries to determine rebar lengths. For instance, the column height in Figure 18 is set as the lengths of vertical rebar.

$$sim\left(X^M, X^G\right) = X^M \cdot X^G \Big/ \left(\left\|X^M\right\| \left\|X^G\right\|\right) = 0.99 \quad (10)$$

IEEE *Access*

Z. Xiang et al.: Integrated Framework for BIM Development of Concrete Buildings Containing Both Surface Elements and Rebar
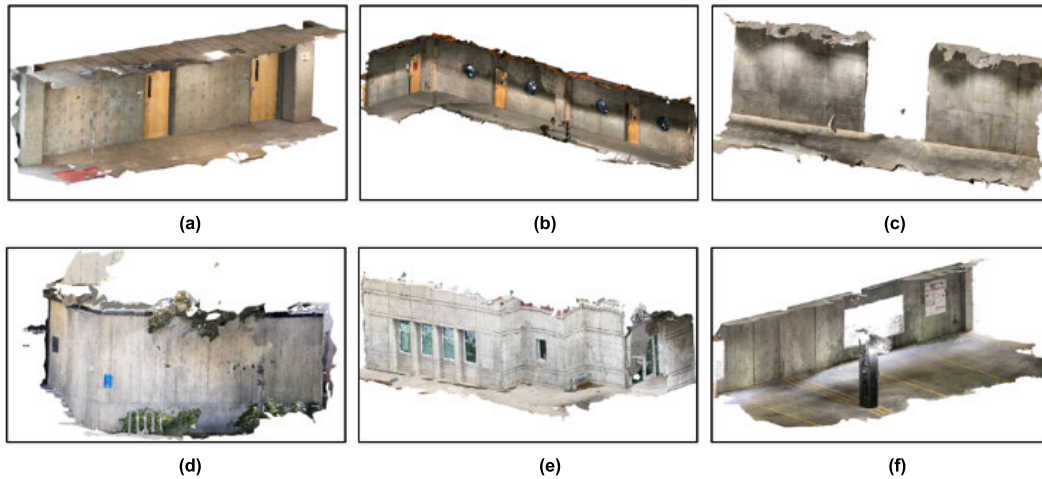
FIGURE 12. Point clouds: (a) Case 1, (b) Case 2, (c) Case 3, (d) Case 4, (e) Case 5, and (f) Case 6.
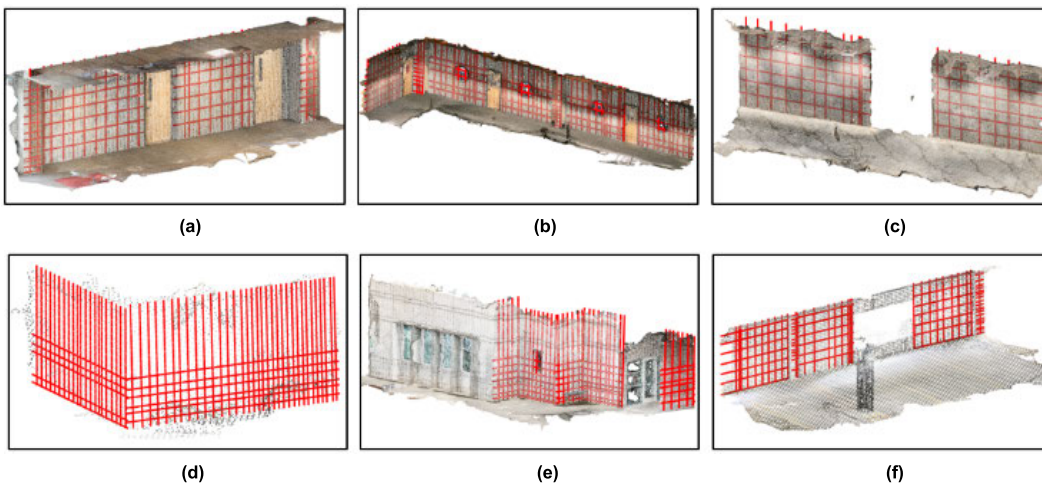

FIGURE 13. Point clouds Inserted with Rebar: (a) Case 1, (b) Case 2, (c) Case 3, (d) Case 4, (e) Case 5, and (f) Case 6.
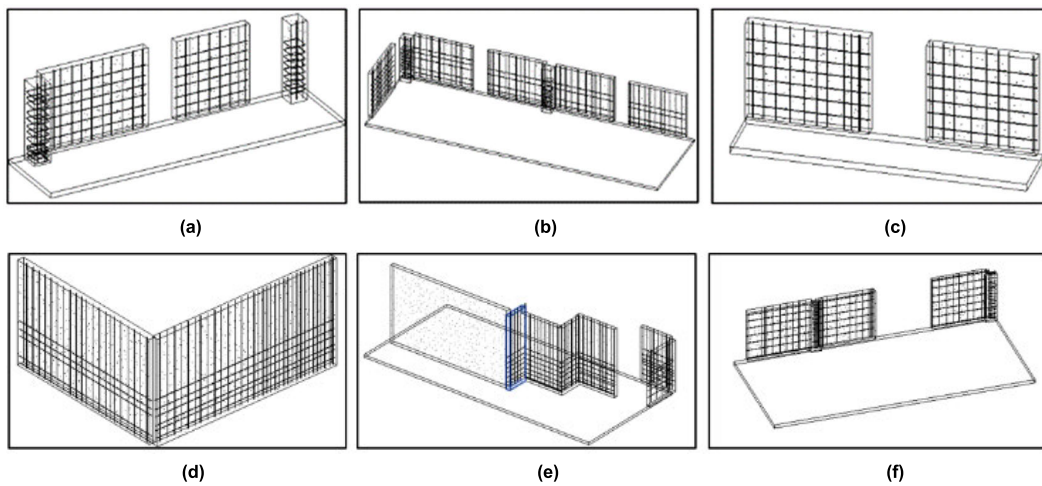

FIGURE 14. As-built BIM: (a) Case 1, (b) Case 2, (c) Case 3, (d) Case 4, (e) Case 5, and (f) Case 6.

D. LIMITATIONS

Although rebar has been successfully translated from GPR data into corresponding elements in BIMs for in-service buildings, a number of limitations still exist:

The intuitive approach to evaluate the performance of rebar placement is to compare the rebar locations between BIM and actual concrete elements, but there is one major obstacle that the construction error exists and causes the deviation between

Z. Xiang et al.: Integrated Framework for BIM Development of Concrete Buildings Containing Both Surface Elements and Rebar

IEEE *Access*
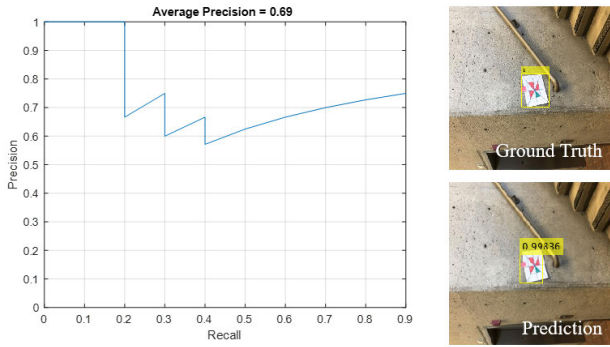
FIGURE 15. Faster RCNN performance on the testing dataset.

FIGURE 16. Three examples of recognized labels by using Faster RCNN.
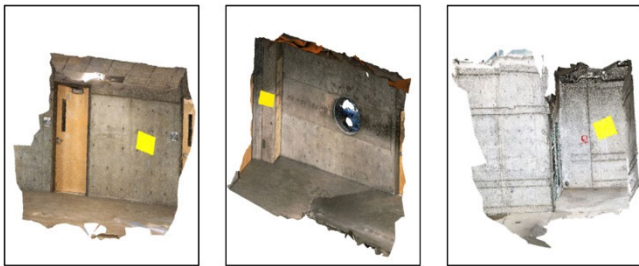
FIGURE 17. Three examples of indicating labels in 3D models.
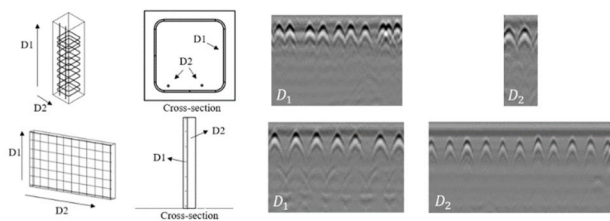
FIGURE 18. Rebar placement in columns and walls.

actual locations and drawings. For instance, as shown in drawings, the distances between the vertical rebar in the left wall of Case 2 (Figure 12b) are the same as 300mm, but the determined distances vary from 262.5mm ∼ 357.5mm. Thus, it is difficult to directly compare the rebar locations between BIM and concrete buildings. Even though these errors can be controlled within an acceptable range by adopting proper methods, errors are always presented in as-built BIMs and cannot be avoided. One potential solution is to design an
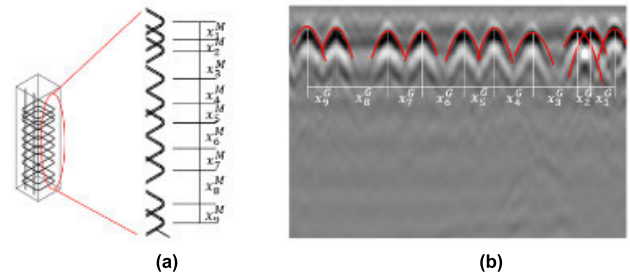
FIGURE 19. Distance comparison between rebars: (a) BIM model and (b) GPR data.

experimental concrete element that can accurately control the locations of all rebar.

Another limitation of this research is that some openings in walls (Figures 13b and 13e) are not considered when placing rebar. This phenomenon is caused in the procedure of as-built BIM development that our method fails to detect these windows or windows are too small to be identified in walls. In this case, rebar pass through windows by extending the detected rebars in the walls beneath or above windows. To solve this issue, the improvement of involving these windows should be considered during as-built BIM development.

V. CONCLUSION AND FUTURE WORKS

Developing as-built BIM with surface elements (e.g., column, shear wall, and slab) and rebar is a challenging task that needs to address the issues of automated element identification, accurate rebar localization, and efficient rebar placement. Although these issues have been explored individually, to the best of our knowledge, there have been no prior studies to develop integrated systems to address these issues together. In this research, we proposed an automated framework that can develop as-built BIM for in-service buildings with surface elements and rebar by using GPR. To achieve this goal, we (1) developed an as-built BIM with the inverse photogrammetry method and a deep learning approach and (2) identified rebar from GPR data with the frequency filter-based method and a rebar depth determination method. Then, a label has been designed to attach to scanned elements, and Faster RCNN was utilized to automatically recognize labels. Meanwhile, timestamps were adopted to link the GPR data and the labeled images for mapping rebars from GPR data into corresponding elements in BIMs. The *IFC schema* was deployed to generate as-built BIMs that were compatible with various BIM platforms. Finally, six case studies were selected to evaluate the proposed framework. By updating the datasets used for training the DeepLab in the step of BIM development and Faster RCNN for label identification, our proposed workflow can be applied to other cases. The results are promising and can draw two major conclusions:

1) Using timestamps and labeled images to connect GPR data and BIMs is a successful setting that all rebars are translated from GPR data into corresponding elements in BIMs. Meanwhile, Faster RCNN is an efficient tool to recognize labels from massive images as the accuracy can reach 100%.

IEEE *Access*

Z. Xiang et al.: Integrated Framework for BIM Development of Concrete Buildings Containing Both Surface Elements and Rebar

2) Developing as-built BIM by using the proposed framework is completely automated and compatible with various BIM platforms due to the application of *IFC*. The rebar can be inserted into the corresponding element from GPR data with accurate coordinates.

As part of the future research plans, the authors will consider more diverse element categories (i.e., all possible shapes and cross sections of columns, etc.). Developing an integrated hardware setting, capable of handling the tasks of GPR and digital cameras simultaneously, will be another future research task.

REFERENCES

[1] S. Tang, D. R. Shelden, C. M. Eastman, P. Pishdad-Bozorgi, and X. Gao, "A review of building information modeling (BIM) and the Internet of Things (IoT) devices integration: Present status and future trends," *Automat. Construct.*, vol. 101, pp. 127–139, May 2019, doi: 10.1016/j.autcon.2019.01.020.

[2] X. Zhao, "A scientometric review of global BIM research: Analysis and visualization," *Autom. Construct.*, vol. 80, pp. 37–47, Aug. 2017, doi: 10.1016/j.autcon.2017.04.002.

[3] ValuatesReports. *Building Information Modeling (BIM) Market Size Worth Value Report: Valuates Reports*. Accessed: May 5, 2021. [Online]. Available: https://reports.valuates.com/market-reports/360I-Auto-0Y68/building-information-modeling

[4] M. Bassier and M. Vergauwen, "Unsupervised reconstruction of building information modeling wall objects from point cloud data," *Autom. Construct.*, vol. 120, Dec. 2020, Art. no. 103338, doi: 10.1016/j.autcon.2020.103338.

[5] R. Charef, H. Alaka, and S. Emmitt, "Beyond the third dimension of BIM: A systematic review of literature and assessment of professional views," *J. Building Eng.*, vol. 19, pp. 242–257, Sep. 2018, doi: 10.1016/j.jobe.2018.04.028.

[6] R. Charef, S. Emmitt, H. Alaka, and F. Fouchal, "Building information modelling adoption in the European union: An overview," *J. Building Eng.*, vol. 25, Sep. 2019, Art. no. 100777, doi: 10.1016/j.jobe.2019.100777.

[7] H.-L. Chi, M.-K. Kim, K.-Z. Liu, J. P. P. Thedja, J. Seo, and D.-E. Lee, "Rebar inspection integrating augmented reality and laser scanning," *Autom. Construct.*, vol. 136, Apr. 2022, Art. no. 104183, doi: 10.1016/j.autcon.2022.104183.

[8] X. Yuan, A. Smith, F. Moreu, R. Sarlo, C. D. Lippitt, M. Hojati, S. Alampalli, and S. Zhang, "Automatic evaluation of rebar spacing and quality using LiDAR data: Field application for bridge structural assessment," *Autom. Construct.*, vol. 146, Feb. 2023, Art. no. 104708, doi: 10.1016/j.autcon.2022.104708.

[9] Q. Wang, J. C. P. Cheng, and H. Sohn, "Automated estimation of reinforced precast concrete rebar positions using colored laser scan data," *Comput.-Aided Civil Infrastruct. Eng.*, vol. 32, no. 9, pp. 787–802, Sep. 2017, doi: 10.1111/mice.12293.

[10] Z. Xiang, G. Ou, and A. Rashidi, "Integrated approach to simultaneously determine 3D location and size of rebar in GPR data," *J. Perform. Constr. Facil.*, vol. 34, no. 5, 2020, Art. no. 04020097, doi: 10.1061/(ASCE)CF.1943-5509.0001502.

[11] Z. Xiang, G. Ou, and A. Rashidi, "Automated translation of rebar information from GPR data into as-built BIM: A deep learning-based approach," in *Proc. Comput. Civil Eng. IT Smart Infrastr. Commun.*, Phoenix, AL, USA, Mar. 2021, pp. 374–381.

[12] Z. Xiang, G. Ou, and A. Rashidi, "Robust cascaded frequency filters to recognize rebar in GPR data with complex signal interference," *Autom. Construct.*, vol. 124, Apr. 2021, Art. no. 103593, doi: 10.1016/j.autcon.2021.103593.

[13] A. Rashidi, F. Dai, I. Brilakis, and P. Vela, "Optimized selection of key frames for monocular videogrammetric surveying of civil infrastructure," *Adv. Eng. Informat.*, vol. 27, no. 2, pp. 270–282, Apr. 2013, doi: 10.1016/j.aei.2013.01.002.

[14] Q. Wang and M.-K. Kim, "Applications of 3D point cloud data in the construction industry: A fifteen-year review from 2004 to 2018," *Adv. Eng. Inform.*, vol. 39, pp. 306–319, Jan. 2019, doi: 10.1016/j.aei.2019.02.007.

[15] M. L. Jalón, J. Chiachío, L. M. Gil-Martín, and E. Hernández-Montes, "Probabilistic identification of surface recession patterns in heritage buildings based on digital photogrammetry," *J. Building Eng.*, vol. 34, Feb. 2021, Art. no. 101922, doi: 10.1016/j.jobe.2020.101922.

[16] C. Gong, Y. Song, G. Huang, W. Chen, J. Yin, and D. Wang, "BubDepth: A neural network approach to three-dimensional reconstruction of bubble geometry from single-view images," *Int. J. Multiphase Flow*, vol. 152, Jul. 2022, Art. no. 104100, doi: 10.1016/j.ijmultiphaseflow.2022.104100.

[17] S. D. Geyter, J. Vermandere, H. D. Winter, M. Bassier, and M. Vergauwen, "Point cloud validation: On the impact of laser scanning technologies on the semantic segmentation for BIM modeling and evaluation," *Remote Sens.*, vol. 14, no. 3, p. 582, Jan. 2022, doi: 10.3390/rs14030582.

[18] Y. Xu, X. Tong, and U. Stilla, "Voxel-based representation of 3D point clouds: Methods, applications, and its potential use in the construction industry," *Autom. Construct.*, vol. 126, Jun. 2021, Art. no. 103675, doi: 10.1016/j.autcon.2021.103675.

[19] I. Brilakis, H. Fathi, and A. Rashidi, "Progressive 3D reconstruction of infrastructure with videogrammetry," *Autom. Construct.*, vol. 20, no. 7, pp. 884–895, 2011, doi: 10.1016/j.autcon.2011.03.005.

[20] F. Dai, A. Rashidi, and I. V. P. Brilakis, "Comparison of image-based and time-of-flight-based technologies for three-dimensional reconstruction of infrastructure," *J. Constr. Eng. Manag.*, vol. 139, no. 1, pp. 69–79, 2013, doi: 10.1061/(ASCE)CO.1943-7862.0000565.

[21] *Handbook of Optical and Laser Scanning*, Taylor & Francis, London, U.K., 2012, p. 788.

[22] R. Farid and C. Sammut, "A relational approach to plane-based object categorization," in *Proc. RSS Workshop RGB-D Cameras*, Jul. 2012, pp. 1–8.

[23] P. H. Torr and A. Zisserman, "Robust parameterization and computation of the trifocal tensor," *Image Vis Comput.*, vol. 15, no. 8, pp. 591–605, 1997, doi: 10.1016/S0262-8856(97)00010-3.

[24] X. Ning, X. Zhang, Y. Wang, and M. Jaeger, "Segmentation of architecture shape information from 3D point cloud," in *Proc. 8th Int. Conf. Virtual Reality Continuum Appl. Ind.*, Dec. 2009, pp. 127–132.

[25] Q. Zhan, Y. Liang, and Y. Xiao, "Color-based segmentation of point clouds," *Laser Scanning*, vol. 38, no. 3, pp. 155–161, 2009.

[26] A. Kazi, A. Sausthanmath, S. V. Gurlahosur, and U. Kulkarni, "Detection of holes in 3D architectural models using shape classification based bubblegum algorithm," *Proc. Comput. Sci.*, vol. 167, pp. 1684–1695, Jan. 2020, doi: 10.1016/j.procs.2020.03.379.

[27] D. Kong, L. Xu, and X. Li, "A new method for building roof segmentation from airborne LiDAR point cloud data," *Meas. Sci. Technol.*, vol. 24, no. 9, Sep. 2013, Art. no. 095402, doi: 10.1088/0957-0233/24/9/095402.

[28] F. Xue, W. Lu, Z. Chen, and C. J. Webster, "From LiDAR point cloud towards digital twin city: Clustering city objects based on gestalt principles," *ISPRS J. Photogramm. Remote Sens.*, vol. 167, pp. 418–431, Sep. 2020, doi: 10.1016/j.isprsjprs.2020.07.020.

[29] L. Li, J. Yao, J. Tu, X. Liu, Y. Li, and L. Guo, "Roof plane segmentation from airborne LiDAR data using hierarchical clustering and boundary relabeling," *Remote Sens.*, vol. 12, no. 9, p. 1363, Apr. 2020, doi: 10.3390/rs12091363.

[30] C. Thomson and J. Boehm, "Automatic geometry generation from point clouds for BIM," *Remote Sens.*, vol. 7, no. 9, pp. 11753–11775, Sep. 2015, doi: 10.3390/rs70911753.

[31] C. Wang, Y. K. Cho, and C. Kim, "Automatic BIM component extraction from point clouds of existing buildings for sustainability applications," *Autom. Construct.*, vol. 56, pp. 1–13, Aug. 2015, doi: 10.1016/j.autcon.2015.04.001.

[32] L. Díaz-Vilariño, B. Conde, S. Lagüela, and L. Henrique, "Automatic detection and segmentation of columns in as-built buildings from point clouds," *Remote Sens.*, vol. 7, no. 11, pp. 15651–15667, 2015, doi: 10.3390/rs71115651.https://doi.org/

[33] I. Anagnostopoulos, V. Pătrăucean, I. Brilakis, and P. Vela, "Detection of walls, floors, and ceilings in point cloud data," in *Proc. Construct. Res. Congr.*, May 2016, pp. 2302–2311.

[34] R. Romero-Jarén and J. J. Arranz, "Automatic segmentation and classification of BIM elements from point clouds," *Autom. Construct.*, vol. 124, Apr. 2021, Art. no. 103576, doi: 10.1016/j.autcon.2021.103576.

[35] J. Xue, X. Hou, and Y. Zeng, "Rough registration of BIM element projection for construction progress tracking," *IEEE Access*, vol. 10, pp. 8305–8316, 2022, doi: 10.1109/ACCESS.2022.3144150.

[36] J. Jung, C. Stachniss, S. Ju, and J. Heo, "Automated 3D volumetric reconstruction of multiple-room building interiors for as-built BIM," *Adv. Eng. Informat.*, vol. 38, pp. 811–825, Oct. 2018, doi: 10.1016/j.aei.2018.10.007.

Z. Xiang et al.: Integrated Framework for BIM Development of Concrete Buildings Containing Both Surface Elements and Rebar

IEEE Access

[37] R. Lu, I. Brilakis, and C. R. Middleton, "Detection of structural components in point clouds of existing RC bridges," *Comput.-Aided Civil Infrastruct. Eng.*, vol. 34, no. 3, pp. 191–212, Mar. 2019, doi: 10.1111/mice.12407.

[38] W. W.-L. Lai, X. Dérobert, and P. Annan, "A review of ground penetrating radar application in civil engineering: A 30-year journey from locating and testing to imaging and diagnosis," *NDT&E Int.*, vol. 96, pp. 58–78, Jun. 2018, doi: 10.1016/j.ndteint.2017.04.002.

[39] D. J. Daniels, *Ground Penetrating Radar*, 2nd ed. London, U.K.: The Institution of Electrical Engineers, 2004.

[40] Z. Xiang, A. Rashidi, and G. G. Ou, "States of practice and research on applying GPR technology for labeling and scanning constructed facilities," *J. Perform. Constr. Facil.*, vol. 33, no. 5, 2019, Art. no. 03119001, doi: 10.1061/(ASCE)CF.1943-5509.0001313.

[41] W. Lei, F. Hou, J. Xi, Q. Tan, M. Xu, X. Jiang, G. Liu, and Q. Gu, "Automatic hyperbola detection and fitting in GPR B-scan image," *Autom. Construct.*, vol. 106, Oct. 2019, Art. no. 102839, doi: 10.1016/j.autcon.2019.102839.

[42] M.-T. Pham and S. Lefevre, "Buried object detection from B-scan ground penetrating radar data using faster-RCNN," in *Proc. IEEE Int. Geosci. Remote Sens. Symp.*, Jul. 2018, pp. 6804–6807.

[43] S. Gibb and H. M. La, "Automated rebar detection for ground-penetrating radar," in *Proc. Int. Symp. Vis. Comput.*, Cham, Switzerland: Springer, Dec. 2016, pp. 815–824.

[44] P. Kaur, "Automated GPR rebar analysis for robotic bridge deck evaluation," *IEEE Trans. Cybern.*, vol. 46, no. 10, pp. 2265–2276, May 2015, doi: 10.1109/TCYB.2015.2474747.

[45] Q. Dou, L. Wei, D. R. Magee, and A. Cohn, "Real-time hyperbola recognition and fitting in GPR data," *IEEE Trans. Geosci. Remote Sens.*, vol. 55, no. 1, pp. 51–62, Jan. 2017, doi: 10.1109/TGRS.2016.2592679.

[46] F. Zhou, Z. Chen, H. Liu, J. Cui, B. Spencer, and G. Fang, "Simultaneous estimation of rebar diameter and cover thickness by a GPR-EMI dual sensor," *Sensors*, vol. 18, no. 9, p. 2969, Sep. 2018, doi: 10.3390/s18092969.

[47] J. H. Bungey, "Sub-surface radar testing of concrete: A review," *Construct. Building Mater.*, vol. 18, no. 1, pp. 1–8, Feb. 2004, doi: 10.1016/S0950-0618(03)00093-X.

[48] P. Wiwatrojanagul, R. Sahamitmongkol, S. Tangtermsirikul, and N. Khamsemanan, "A new method to determine locations of rebars and estimate cover thickness of RC structures using GPR data," *Construct. Building Mater.*, vol. 140, pp. 257–273, Jun. 2017, doi: 10.1016/j.conbuildmat.2017.02.126.

[49] K. Agred, G. Klysz, and J.-P. Balayssac, "Location of reinforcement and moisture assessment in reinforced concrete with a double receiver GPR antenna," *Construct. Building Mater.*, vol. 188, pp. 1119–1127, Nov. 2018, doi: 10.1016/j.conbuildmat.2018.08.190.

[50] K. J. Cho and J. H. Lee, "An efficient algorithm for rebar element generation using 3D CAD data," *J. Comput. Struct. Eng. Inst. Korea*, vol. 22, no. 5, pp. 475–485, 2009.

[51] Z. Xiang, A. Rashidi, and G. Ou, "Automated framework to translate rebar spatial information from GPR into BIM," *J. Constr. Eng. Manag.*, vol. 147, no. 10, 2021, Art, no. 04021120, doi: 10.1061/(ASCE)CO.1943-7862.0002141.

[52] Y. Byun and B.-S. Sohn, "ABGS: A system for the automatic generation of building information models from two-dimensional CAD drawings," *Sustainability*, vol. 12, no. 17, p. 6713, Aug. 2020, doi: 10.3390/su12176713.

[53] Q. Wang, Y. Tan, and Z. Mei, "Computational methods of acquisition and processing of 3D point cloud data for construction applications," *Arch. Comput. Methods Eng.*, vol. 27, pp. 479–499, Apr. 2020, doi: 10.1007/s11831-019-09320-4.

[54] R. Subbarao and P. Meer, "Beyond RANSAC: User independent robust regression," in *Proc. Conf. Comput. Vis. Pattern Recognit. Workshop (CVPRW)*, Jun. 2006, p. 101.

[55] R. S. Likes, "Moving gradient zeugmatography," U.S. Patent 4 307 343, Dec. 22, 1981.

[56] R. Mezrich, "A perspective on K-space," *Radiology*, vol. 195, no. 2, pp. 297–315, May 1995, doi: 10.1148/radiology.195.2.7724743.

[57] K. Dinh, N. Gucunski, J. Kim, and T. H. Duong, "Understanding depth-amplitude effects in assessment of GPR data from concrete bridge decks," *NDT E Int.*, vol. 83, pp. 48–58, Oct. 2016, doi: 10.1016/j.ndteint.2016.06.004.

[58] A. Braun and A. Borrmann, "Combining inverse photogrammetry and BIM for automated labeling of construction site images for machine learning," *Autom. Construct.*, vol. 106, Oct. 2019, Art. no. 102879, doi: 10.1016/j.autcon.2019.102879.

[59] J. Weng, P. Cohen, and M. Herniou, "Camera calibration with distortion models and accuracy evaluation," *IEEE Trans. Pattern Anal. Mach. Intell.*, vol. 14, no. 10, pp. 965–980, Oct. 1992, doi: 10.1109/34.159901.

ZHONGMING XIANG received the B.S. degree in theoretical and applied mechanics from Sun Yat-sen University, Guangzhou, China, in 2013, and the Ph.D. degree in civil and environmental engineering from The University of Utah, Salt Lake City, UT, USA, in 2021. He is currently a Transmission Line Engineer at Stantec Consulting Service Inc. His research interests include full-scale 3D reconstruction for infrastructures, nondestructive testing with radar images, and power line system resilience improvement.

GE OU received the B.S. degree in theoretical and applied mechanics from the Harbin Institute of Technology, Harbin, China, in 2010, the B.E. degree in civil engineering from the University of Sydney, Sydney, Australia, in 2010, and the Ph.D. degree in civil engineering from Purdue University, West Lafayette, IN, USA, in 2016. She is currently an Assistant Professor at the Department of Civil and Coastal Engineering, University of Florida. Her research is inspired by the community-centered informed hazard-oriented decision-making, which lead to the development of high fidelity and computational efficient regional-scale simulation platform. Her research interests include physical and surrogate modeling of complex civil infrastructure systems, machine learning, information theory, advanced experimental testing, model updating, and the integration of data analytics with physical-based modeling.

ABBAS RASHIDI (Member, IEEE) received the M.S. degree in civil and environmental engineering from Tehran Polytechnic, in 2004, and the M.S. degree in electrical and computer engineering and the Ph.D. degree in civil and environmental engineering from Georgia Tech, in 2013 and 2014, respectively.

His dual background in civil engineering and electrical and computer engineering, has enabled him to conduct multidisciplinary research and to implement electrical engineering tools and computational techniques to solve complex civil engineering problems. In particular, he is interested in applying audio/image/video processing techniques to analyze and model complex civil engineering systems. He currently serves as a member for several professional committees, including the Signal Processing in Acoustics Committee of the Acoustical Society of America and the Data Sensing and Analysis (DSA) Committee of the American Society of Civil Engineers (ASCE). He is an Associate Editor and a member of the Editorial Board of two ASCE journals, such as *Journal of Construction Engineering and Management* (ASCE) and *Journal of Performance of Constructed Facilities* (ASCE).

• • •